ACS Catalysis

pubs.acs.org/acscatalysis Research Article

Role of Water on Zeolite-Catalyzed Dehydration of Polyalcohols and EVOH Polymer

Han K. Chau, Quy P. Nguyen, Ana Carolina Jerdy, Dai-Phat Bui, Lance L. Lobban, Bin Wang, and Steven P. Crossley*

Cite This: *ACS Catal.* 2023, 13, 1503−1512 Read Online

ACCESS | Metrics & More | Article Recommendations | Supporting Information

ABSTRACT: Selective dehydration of polyalcohols over zeolites containing Brønsted acids is a promising approach to purify and recycle multilayer polymer films consisting of non-polar polymers such as polyethylene and polar polymers like ethylene−vinyl alcohol copolymer. In addition, polar aprotic solvents can be utilized to improve the diffusion of polymer molecules to access the active sites in solid catalysts. Here, we reveal the positive role of water on dehydration of ethylene−vinyl alcohol polymer over a solid acid catalyst in the presence of γ-valerolactone as the solvent. Through vapor-phase experiments with 2,5-hexanediol as a model compound and theoretical calculations, we reveal that water facilitates dehydration reactions by delocalizing surface-bound protons and allowing dehydration rates to occur even in the presence of solvents that would otherwise inhibit reaction rates. The hydronium ion clusters act as delocalized acid sites, leading to improved surface coverage of the reactant, and consequently enhance dehydration activity in the presence of solvent molecules. This example of co-solvent-induced modulation of environments around active sites could open doors for polymer recycling and upcycling.

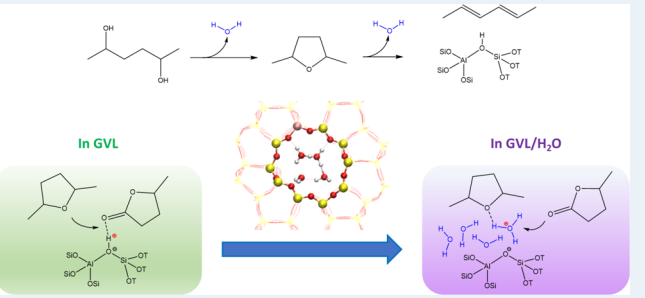

KEYWORDS: *polymer upcycling, zeolites, dehydration, water effect, competitive adsorption*

1. INTRODUCTION

Plastics play a vital part in modern life due to their outstanding durability, versatility, lightweight nature, and cost efficiency. Recently, multilayer packaging materials have been advancing rapidly and emerging as a desirable choice for protecting perishable foods and medicine due to their excellent moisture resistance and oxygen barrier properties with less material and energy required for production than single-resin plastic alternatives.[1] The sharp increase in the consumption of these plastic products creates significant challenges in plastic recycling, yet it provides opportunities for developing feasible catalytic systems for the recycling of plastic waste.[2,3] At present, most plastic waste ends up in landfills, thus losing the intrinsic value of the material while creating environmental concerns. In recent years, besides conventional mechanical methods, many chemical processes and catalytic systems such as pyrolysis, hydrogenolysis, and solvolysis have been proposed to recycle plastic waste and convert them into high-value products, which foster a circular economy for plastics.[4−11] Recycling of mixed polymers or multilayer films is even more challenging due to the presence of different non-polar polymers such as polyethylene and polypropylene and polar polymers like ethylene−vinyl alcohol copolymer (EVOH).[2,12] The ability to selectively target specific polymers in these multicomponent mixtures would enable vastly improved recycling. A staged conversion would allow for purification and reuse or alternatively better optimized post-processing approaches to yield higher-value products such as olefin monomers, fuels, and lubricants. Huber and co-workers have proposed a non-catalytic dissolution and precipitation approach for the recycling of multilayer plastic films, which requires the considerable usage of multiple different polar and non-polar solvents.[13,14] The approach proposed here illustrates a similar concept, but with a prior catalytic treatment rather than solvent treatment alone.

Alcohol dehydration over solid acid catalysts such as zeolites has been studied extensively for decades, especially in biomass upgrading processes.[15−17] Since zeolites contain both Brønsted and Lewis acid sites, different proposals have been made regarding the kinetically relevant active site in alcohol dehydration reactions. However, it is generally accepted that the alcohol dehydration rate correlates well with the Brønsted acid site (BAS) density in zeolite catalysts.[18] Water is the byproduct of alcohol dehydration reactions and may modify activity as well. Lercher and co-workers reported that the

Received: October 27, 2022
Revised: December 20, 2022
Published: January 10, 2023

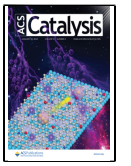

presence of water molecules inside zeolite pores around BASs could facilitate proton delocalization and form hydronium ion clusters, which can act as mobile acid sites and generate a highly ionic environment inside zeolite pores for cyclohexanol dehydration in the aqueous phase.[19−21] On the other hand, the presence of water in the dehydration of alkanols (e.g., ethanol, propanol, and butanol) has also been reported to inhibit dehydration rates by stabilizing adsorbed intermediates and forming stable dimers, alcohol−water clusters, and extended hydrogen-bonded networks in the confined environment of microporous zeolites.[16,18,22,23] However, it is unclear what influence water will have during the dehydration of EVOH polar polymers in the complex environment that is created in the presence of a polar aprotic solvent.

Here, we carry out the dehydration of 2,5-hexanediol (the model compound) and real EVOH polymers over Brønsted-acid zeolites in the presence of a polar aprotic solvent. A unique feature of this approach is that the polar polymer can be converted to a non-polar polymer, which is more compatible with the other polyolefins and allows a more efficient recycling of the multilayer polymer films, without breaking the C−C bonds of the polymer backbone. γ-Valerolactone (GVL), a sustainable green solvent derived from lignocellulosic biomass,[24] was used to improve the accessibility of polymer molecules to the active sites on solid catalysts with a lower temperature requirement compared to molten-phase reactions. We report the reduced dehydration rate due to the competitive adsorption of the polar aprotic solvent, which can be alleviated by co-feeding water. Kinetics and mechanistic investigations suggest that in the presence of water, hydronium ion clusters are more favorable to reactant adsorption than are the framework BASs.

2. EXPERIMENTAL SECTION

2.1. Reagents. Poly(vinyl alcohol-*co*-ethylene) (EVOH, ethylene 32 mol %, M_n = 16,202 Da estimated by ^{1}H NMR) in pellet form was purchased from Sigma-Aldrich and was cryogenically ground to obtain fine powder form. 2,5-Hexanediol (99%, mixture of isomers, Sigma-Aldrich), GVL (≥99%, Sigma-Aldrich), 2,5-dimethyltetrahydrofuran (DMTHF, mixture of cis and trans, 96%, Sigma-Aldrich), 2,4-hexadiene (mixture of isomers, 90%, Sigma-Aldrich), 1,5-hexadiene (97%, Sigma-Aldrich), *n*-hexane (99%, Sigma-Aldrich), 1-hexene (97%, Sigma-Aldrich), and 4-pentenoic acid (97%, Sigma-Aldrich) were obtained from the commercial supplier and used as received.

2.2. Catalyst Preparation. ZSM-5 zeolites with three different Si/Al ratios were purchased in the ammonium form NH_4-ZSM-5 from Zeolyst International (CBV-5524G with Si/Al = 25, CBV-8014 with Si/Al = 40, CBV-28014 with Si/Al = 140). Beta zeolite (Si/Al = 133) was obtained in proton-form H-Beta from Alfa Aesar. Sodium exchange of NH_4-ZSM-5 (CBV-8014 and CBV-28014) was carried out to titrate a fraction of the BASs. NH_4-ZSM-5 (CBV-8014) and NH_4-ZSM-5 (CBV-28014) samples were mixed with 0.5 M $NaNO_3$ solution and 10 mM $NaNO_3$ solution, respectively, with the ratio of 20 mL solution per gram catalyst. Deionized water and commercial $NaNO_3$ (Sigma-Aldrich, ACS Reagent, ≥99.0%) were used to prepare $NaNO_3$ solution. The mixture of NH_4-ZSM-5 powder and $NaNO_3$ solution was stirred for 12 h at room temperature. Then, the mixture was centrifuged, and the solid part was washed five times with deionized water, followed by a drying step at 80 °C in a vacuum oven for 24 h.

All catalyst samples (except beta zeolite in proton form) were calcined in flowing dry air with the ramping rate of 2 °C/min up to 600 °C and kept at that temperature for 5 h to obtain proton-form H-ZSM-5. Protonated zeolites were then pelletized, crushed, and sieved to particles with sizes ranging from 90 to 250 μm. H-ZSM-5 zeolites with Si/Al = 25, Si/Al = 40, and Si/Al = 140 and sodium-titrated samples are denoted as MFI-25, MFI-40, MFI-140, Na-MFI-40, and Na-MFI-140, respectively. H-Beta zeolite (Si/Al = 133) is denoted as BEA-133.

2.3. Characterization. Temperature-programmed reaction (TPRx) of isopropylamine (IPA) coupled with an MKS Cirrus 200 quadrupole mass spectrometer was carried out on catalyst samples to determine BAS densities of these catalysts. The details of this method are described elsewhere.[25]

Thermogravimetric analysis (TGA) was performed on a Netzsch STA 449F1 equipped with a pin thermocouple and a Netzsch nano-balance to quantify the number of water molecules per acid site in MFI-140. The catalyst was dried by heating up to 300 °C with the ramping rate of 10 °C/min and kept for 1 h in flowing helium (125 mL/min) before introducing water at 3.5 kPa in a flow reactor. Then the catalyst was transferred to the crucible and heated from 40 to 600 °C at the ramp rate of 5 °C/min in flowing argon (20 mL/min). The number of water molecules per BAS in MFI-140 was quantified based on the desorption of water from the catalyst indicated by the weight loss of the sample and the BAS density from IPA-TPRx experiments.

Fourier-transform infrared (FT-IR) spectroscopy was carried out on a PerkinElmer Spectrum 100 FT-IR spectrometer equipped with a high-temperature diffuse reflectance infrared Fourier transformation CaF_2 cell (HVC, Harrick). A blank run of KBr pellet was obtained for the background. The solid samples were pretreated as described below before obtaining FT-IR spectra in a He inert atmosphere.

Nuclear magnetic resonance (NMR) experiments were performed at the OU NMR Facility on a Varian VNMRS 400 MHz spectrometer with a dual broadband probe at 25 °C to estimate the molecular weight of EVOH. NMR samples were prepared in DMSO-d_6 solvent.

2.4. Catalytic Testing. Dehydration of EVOH was carried out in a PTFE bottle in a nitrogen atmosphere, which was heated by a silicon oil bath. EVOH fine powder and the solvent were stirred and heated to the reaction temperature before adding the catalyst and starting the reaction. The reaction mixture was stirred with PTFE magnetic stir bar at 600 rpm in all experiments. After the reaction, the product was filtered to separate the liquid and solid parts. The liquid part was analyzed by gas chromatography−mass spectrometry (GC−MS) and showed no conversion of solvent under the reaction conditions. The solid part was washed with deionized water and dried in a vacuum oven at 80 °C overnight to remove the residual solvent before FT-IR analysis.

Vapor-phase flow reactions over zeolite catalysts were conducted in a quartz tube reactor (1/4″ OD) at atmospheric pressure. The catalyst was mixed with acid-washed glass beads and packed between quartz wool layers in the quartz reactor. The quartz reactor was installed inside an oven whose temperature was controlled by a thermocouple inside the quartz reactor and beneath the catalyst bed. Liquid reactants and co-feeding agents were used as received (for DMTHF, deionized water, GVL, 4-pentenoic acid) or diluted in a solvent (for 2,5-hexanediol in GVL, volume ratio 1/16 or 1/5) and

https://doi.org/10.1021/acscatal.2c05303
ACS Catal. 2023, 13, 1503−1512

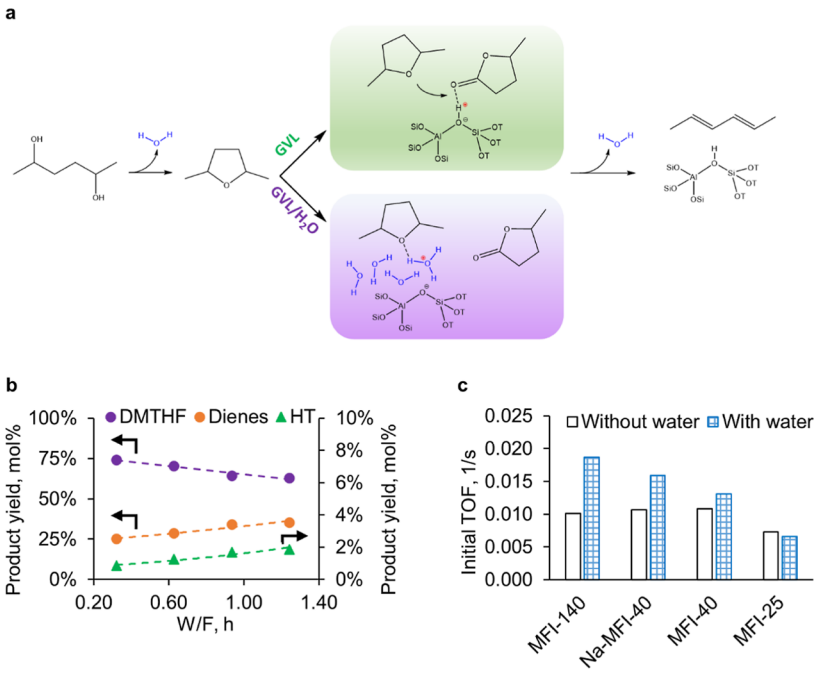

Figure 1. Dehydration of 2,5-hexanediol model compound. (a) Schematic reaction pathway of 2,5-hexanediol dehydration over Brønsted zeolites. (b) Product yields of 2,5-hexanediol dehydration over MFI-140 with varying reaction space time. Reaction conditions: T = 250 °C, $P_{2,5\text{-hexanediol}}$ = 0.09 kPa, P_{GVL} = 0.6 kPa. (c) Initial turnover frequency of hexadiene formation in 2,5-hexanediol dehydration over different H-ZSM-5 zeolites in the absence and presence of water. Reaction conditions: T = 250 °C, $P_{2,5\text{-hexanediol}}$ = 0.09 kPa, P_{GVL} = 0.6 kPa, P_{water} = 0 or 3.5 kPa.

contained in separate gastight syringes which were placed on different syringe pumps. Before injecting reactants, physisorbed water in catalyst samples was removed by heating samples to 300 °C with the ramping rate of 10 °C/min and kept for 1 h in flowing helium (125 mL/min). The oven temperature was then set to reach the desired reaction temperature. Once the reaction temperature reached the set point, reactants were injected to the reactor through septa on a heated vaporization zone using KD Scientific syringe pumps, and the reaction time started to count. To prevent the condensation of reaction products on the downstream tubing, the outlet of the reactor was heated to 250 °C. Samples were collected at different reaction times on stream using a gas sample loop connected with a six-port valve, and products were analyzed using a Hewlett Packard 6890 gas chromatograph equipped with a flame ionization detector and an INNOWax column (30 m × 0.25 mm).

To decouple kinetic effects from catalyst deactivation over reaction time on stream in flow reactions, all reaction rates were extrapolated to zero time on stream to obtain initial rates which are used in reaction order and activation energy plots

$$\text{Reaction space time} = \frac{\text{mass of catalyst (g)}}{\text{reactant flow rate (g/h)}}$$

$$\text{Product yield (mol \%)} = \frac{\text{product flow rate (mol/s)}}{\text{reactant flow rate (mol/s)}} \times 100\%$$

$$\text{Turnover frequency (1/s)} = \frac{\text{molar flow rate of product formed per gram catalyst (mol/g}_{cat}\cdot\text{s)}}{\text{BAS density (mol H}^{+}\text{/g}_{cat}\text{)}}$$

2.5. DFT Calculations. The Vienna ab initio simulation package[26] was used to calculate all electronic energies using density functional theory (DFT). Description of the electron−ion interactions was carried out by the projector-augmented wave[27,28] approach with a plane-wave energy cutoff of 400 eV. The exchange correlation energies were computed by the generalized gradient approximation with Perdew−Burke−Ernzerhof functional.[29] The van der Waals interactions were accounted by using the DFT-D3 semiempirical method.[30] Iteration of self-consistency loops with a convergence level of 10^{-5} to 10^{-7} eV and a maximum atomic force criterion of less than 0.01 eV Å^{-1} were employed to optimize the structures. A literature model for the adsorbate entropy in zeolite[31] was applied to estimate the entropy lost when a gaseous molecule adsorbs into the zeolite pore. For calculations of zero-point energy, the vibrational frequencies at 0 K were obtained by partial Hessian vibrational analysis.[32] The internal energy (U), enthalpy (H), entropy (S), Gibbs free energy (G), and equilibrium constants (K_a) corrected at the reaction conditions were calculated based on the statistical thermodynamics.[33]

A periodic unit cell of H-ZSM5 employed in this paper consists of 96 tetrahedral sites[34] with the lattice constants set to a = 20.078 Å, b = 19.894 Å, and c = 13.372 Å, as in our previous work.[35−37] The BAS was constructed by replacement of a Si atom at a T7 site with one Al atom. The proton was placed in the oxygen bisecting T7 and T8 sites as in our previous work.[35] The molecules in the gas phase were positioned into a cube with the lattice constant of 30 Å.

3. RESULTS AND DISCUSSION

3.1. Effect of the Polar Aprotic Solvent and Co-Feeding Water on Dehydration of the Model Compound. In commercial products, EVOH normally contains about 30 mol % ethylene and 70 mol % vinyl alcohol to maximize the oxygen barrier properties. Therefore, 2,5-hexanediol was selected as the model compound of EVOH to investigate the influence of solvent on dehydration mechanisms. This dialcohol compound has a molar ratio of ethylene to vinyl alcohol similar to that of EVOH, and the

https://doi.org/10.1021/acscatal.2c05303
ACS Catal. 2023, 13, 1503−1512

hydroxyl groups are also located at the secondary carbons like EVOH copolymer.

While the dehydration of diol compounds such as hexanediol over zeolite catalysts has not been adequately addressed in the literature, it is known that hexanediol can undergo a ring-closing reaction to form a cyclic ether, which can then form diolefins by a dehydra-decyclization mechanism. The ring-opening and subsequent dehydration of cyclic ethers such as dimethyl tetrahydrofuran have been extensively studied over solid acid catalysts.[38−42]

The gas-phase dehydration of 2,5-hexanediol with co-feeding GVL over MFI-140 was carried out at 250 °C and atmospheric pressure. The observable products were DMTHF, hexadienes, and hydride-transfer (HT) products (e.g., hexenes). In addition, pentenoic acid (PA) isomers were observed as the products of GVL ring-opening over BASs in MFI-140, which is consistent with the literature.[43] The reaction pathway of 2,5-hexanediol dehydration to form hexadienes over isolated BASs in MFI-140 via a cyclic ether intermediate is shown in Figure 1a, which was identified by varying reaction space time W/F. It should be noted that the conversion of 2,5-hexanediol was 100% during reaction time on stream in these experiments. As shown in Figure 1b, the product yield of DMTHF decreases from 74.0 to 62.9 mol % with increasing W/F from 0.32 to 1.24 h, which suggests that the cyclic ether is the primary product of 2,5-hexanediol dehydration. On the other hand, the yield of hexadienes increases from 25.2 to 35.2 mol % and the yield of HT products increases from 0.8 to 1.8 mol % when the reaction space time increases from 0.32 to 1.24 h, which indicates that these compounds are secondary products.

Additional evidence for this reaction pathway is shown in Figure S1, where product yields were plotted as a function of reaction time on stream over both MFI-140 and MFI-40. Over both catalysts, as the catalyst deactivated during reaction time on stream, the yield of DMTHF increases, while the yield of hexadienes decreases, suggesting reaction in series (i.e., hexanediol → DMTHF → hexadienes). As shown in Figures S1 and S2, the significantly higher yield and rate of formation of DMTHF compared to hexadienes suggests that the formation of cyclic ether intermediate is facile, while the formation of hexadienes is slower. In addition, during a low-temperature (150 °C) experiment shown in Figure S3 in which hexanediol conversion is not complete, the exclusive 100% selectivity to DMTHF strongly suggests that hexadienes are formed as secondary products through the DMTHF primary product.

Because of the significant deactivation that takes place, initial turnover frequencies were used to decouple kinetic effects from catalyst deactivation. Figure S4 shows the best fits for the formation of hexadienes over four different MFI zeolites assuming exponential activity loss, that is, activity given by $TOF = TOF_0 \cdot e^{-\beta t}$. The effect of water on dehydration of 2,5-hexanediol was studied by co-feeding water at a constant partial pressure over different Brønsted zeolites, as shown in Figure 1c, which compares initial TOF in the absence and in the presence of water. The equivalent initial turnover frequencies of hexadiene formation over MFI-140, Na-MFI-40, and MFI-40 in the absence of water are nearly equal. Since these catalysts have identical pore structures (and therefore identical internal mass-transfer characteristics) but different active site densities (given in Table S1), this result suggests that the reactions over these catalysts are not limited by internal diffusion. It is important to point out that hexadiene formation is a secondary product from 2,5-hexanediol dehydration, and the rate of secondary product formation is influenced by sequential reactions. If one interpolates the TOF rates obtained when feeding the ether alone in Figure S15 (interpolated to match the partial pressure of hexanediol fed in Figure 1c), one obtains a TOF value in the absence of co-fed water that is statistically indistinguishable from the TOF obtained when feeding hexanediol when considering the experimental uncertainty as reported in Figures S8 and S9.

On the other hand, the initial turnover frequency over MFI-25, which has the highest acid site density, is lower than that of other MFI catalysts, which implies that the reaction over MFI-25 is likely to be diffusion-limited. Figure 1c shows that in the presence of GVL, the addition of water actually facilitates the dehydration of 2,5-hexanediol to form hexadienes over MFI catalysts operating under a surface-reaction-controlled regime.

A similar effect of water was observed for reaction over high-silica beta zeolite BEA-133 (Figure S5). Interestingly, the effect of water is most pronounced on high-silica H-ZSM-5 zeolite with the lowest acid site density (MFI-140), with the initial turnover frequency of hexadiene formation increasing 85% with co-feeding water. The cause of this increase may be the formation of water molecule clusters and is discussed later in this paper. The rate per gram of catalyst also increases with the addition of water on the three lowest-acid site density catalysts (Figure S6), but over the high-site density MFI-25, the measured rate per gram of catalyst is lower in the presence of water. This decrease could be attributed to the increase of diffusional constraints caused by the presence of the water molecule clusters. It is noted that the BASs in these high-Si/Al zeolites are mainly isolated sites, while the fraction of aluminum in pairs in MFI-40 is about 0.322 based on the Co^{2+} exchange method.[44] Two aluminum atoms separated by two silicon atoms ($AlSi_2Al$ sequence) in zeolites are often considered an aluminum pair.[45] These adjacent sites in zeolite catalysts significantly influence many acid-catalyzed reactions.[46−48] Gounder and co-workers investigated the role of acid site proximity in alkane cracking over chabazite zeolites and found that sodium exchange preferably titrates paired BASs over isolated BASs in CHA frameworks.[49] In our study, the enhancement of the initial rate in the presence of co-fed water over sodium-titrated catalyst Na-MFI-40 (49%) is more significant compared to parent zeolite MFI-40 (21%) as shown in Figure 1c. In addition, the location of BASs in high-silica MFI zeolites (Si/Al > 23) is mainly at the channel intersections.[50] Therefore, the less notable effect of water on higher-acid site density MFI zeolites such as MFI-40 is less likely due to different acid site locations but could be attributed to the acid site distribution or role of site proximity in these catalysts.

It is worth mentioning that the catalysts in this study have a low BAS density with an insignificant amount of extra-framework aluminum species (Figure 2a and Table S1). In addition, the reaction temperature in this study is 250 °C, which is lower than the reported value (450 °C) for dealumination of ZSM-5 zeolites in the presence of water vapor.[51] Therefore, the effect of water here should not be related to the change of zeolite structure under the reaction conditions. On the other hand, the presence of two or more water molecules inside zeolite pores was found to facilitate the delocalization of proton from the zeolite framework and form hydronium ion clusters even at room temperature.[19,20] As shown in Figure 2b, the weight loss of hydrated MFI-140

https://doi.org/10.1021/acscatal.2c05303
ACS Catal. 2023, 13, 1503−1512

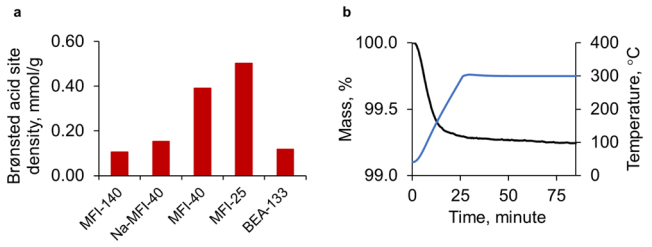

Figure 2. Catalyst characterization. (a) BAS density of different zeolites measured by temperature program reaction of isopropyl amine. (b) Mass loss of MFI-140 sample after being exposed to water (P_{water} = 3.5 kPa, T = 250 °C, 1 h) from TGA.

sample in TGA after being exposed to water under reaction conditions is about 0.76 wt %, leading to the calculated number of 4 water molecules per BAS in MFI-140 catalyst. As a result, the accessibility of the reactant to the hydronium ion clusters or mobile acid sites in the presence of competitive solvent molecules such as GVL can be improved, leading to higher surface coverage and reaction rate.

The influence of partial pressure of water on hexadiene formation over MFI-140 and MFI-40 is shown in Figures S7 and S8. It shows that the effect of water on the turnover frequency of hexadiene formation increases to a maximum value and then plateaus and slowly declines with the increase of the partial pressure of water. This observation suggests that adding a small amount of water (P_{water} = 3.5−6.8 kPa) improves the formation of hexadienes. However, the higher partial pressure of co-fed water may lead to larger hydronium ion clusters that dampen the enhancement effect of water on the dehydration rates over MFI zeolites, possibly due to the hindered accessibility of the reactant to the acid sites.

The presence of water is also known to intervene in the ring-opening of GVL over the solid acid catalyst.[52,53] Haider et al. found that the oxocarbenium ion is stabilized by water, which enables the two-step reaction pathway of GVL ring-opening with lower activation energy.[53] In fact, the formation of PA isomers from GVL ring-opening is enhanced by co-feeding water (Figure S10). PA isomers were found to have a higher heat of adsorption than GVL.[52] Therefore, it is expected that these GVL ring-opening products also inhibit the dehydration of intermediate cyclic ether, as is shown in Figure S11.

Based on these observations, it is important to decouple the role of GVL and water on the dehydration of 2,5-hexanediol over MFI-140. The dehydration pathway of 2,5-hexanediol was found to proceed via intermediate cyclic ether as aforementioned. The kinetic effect of water on alcohol dehydration, the first step in the reaction pathway over solid acid catalysts, has been studied extensively in the literature. Marin et al. found that water does not influence 1-butanol dehydration over ZSM-5 zeolites.[54] On the other hand, a negative effect of water on dehydration rate was observed by Iglesia et al. and Lercher et al., which was explained by the stabilization of adsorption state of alcohol in the presence of water.[16,18] In our studies, this first step is facile and fast, and so the effects of water on the first step cannot be ascertained. However, the water clearly has an effect on the secondary reactions. Therefore, our subsequent studies focused on the effects of water and solvent GVL on the conversion of DMTHF, the primary product of the dialcohol dehydration. Unless otherwise noted, these studies are all carried out over the MFI-140 catalysts, which show the most pronounced effect of co-feeding water.

The results are shown in Figures 3a and S12−S14 for hexadiene formation TOF versus time on stream with

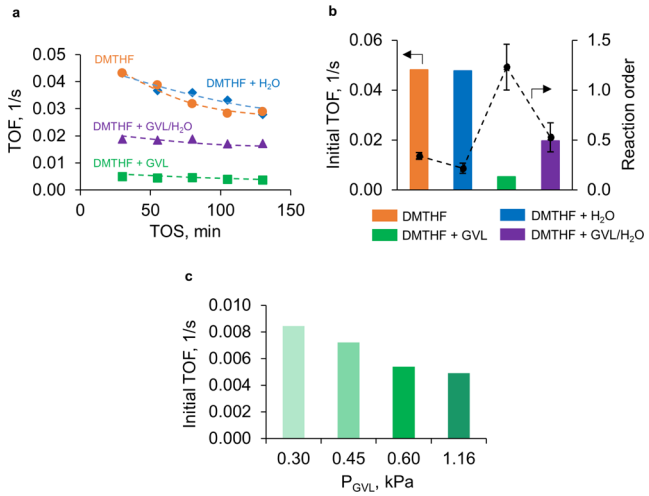

Figure 3. Dehydration of intermediate ether DMTHF. (a) Turnover frequency of hexadiene formation over MFI-140 in the absence and presence of water. Reaction conditions: T = 250 °C, P_{DMTHF} = 0.08 kPa; P_{GVL} = 0 kPa, P_{water} = 0 kPa (orange ●); P_{GVL} = 0 kPa, P_{water} = 3.5 kPa (blue ♦); P_{GVL} = 0.6 kPa, P_{water} = 3.5 kPa (violet ▲); P_{GVL} = 0.6 kPa, P_{water} = 0 kPa (green ■). (b) Correlation between reaction rate and reaction order with respect to DMTHF in different co-feeding experiments over MFI-140. Reaction conditions: T = 250 °C, P_{DMTHF} = 0.08 kPa; P_{GVL} = 0 kPa, P_{water} = 0 kPa (orange ■); P_{GVL} = 0 kPa, P_{water} = 3.5 kPa (blue ■); P_{GVL} = 0.6 kPa, P_{water} = 0 kPa (green ■); P_{GVL} = 0.6 kPa, P_{water} = 3.5 kPa (violet ■). The standard errors are estimated from the least squares method. (c) Inhibition effect of GVL on dehydration of DMTHF over MFI-140. Reaction conditions: T = 250 °C, P_{DMTHF} = 0.08 kPa, P_{GVL} = 0.30−1.16 kPa.

DMTHF as the reactant. As was the case when hexanediol was the fed reactant, several observations can be made: the addition of solvent GVL significantly inhibits the rate; co-feeding water in the absence of GVL has a minor effect, but co-feeding water in the presence of GVL enhances the rate over that occurring with only GVL co-fed. The turnover frequencies of hexadiene formation over MFI-140 and Na-MFI-140 are identical and higher than that over MFI-40 (Figures S12−S14), indicating that the DMTHF dehydration in the absence of GVL over MFI-140 is surface reaction-controlled, while the DMTHF dehydration in the absence of GVL over MFI-40 is likely diffusion-limited. Deactivation does occur, so as before, the data are fit to a simple deactivation model to obtain initial TOF values to aid in subsequent analysis of reaction mechanism and kinetics. The dependence of hexadiene formation rate on DMTHF partial pressure was obtained by varying DMTHF partial pressure for several cases: no co-fed components (Figure S15), with co-fed water (Figure S16), with co-fed GVL (Figure S17), and with co-fed water and GVL (Figure S18). The resulting reaction orders are presented in Figure 3b, along with the initial TOF for P_{DMTHF} = 0.08 kPa. The similar turnover frequency and reaction order of DMTHF with and without co-feeding water indicate that water influences the adsorption state and transition state of the vapor-phase dehydration of DMTHF in the absence of an organic solvent to the same extent which does not change the intrinsic energy barrier. On the other hand, adding GVL significantly reduces the dehydration of DMTHF. Further-

https://doi.org/10.1021/acscatal.2c05303
ACS Catal. 2023, 13, 1503−1512

more, the presence of water mitigates the inhibition effect of GVL and improves the formation of hexadienes when the reaction is carried out in the presence of GVL. Therefore, this result on the intermediate ether could explain well the observation rate enhancements upon introduction of water enhancement for 2,5-hexanediol dehydration over MFI-140 (Figure 1c).

The inhibition effect of GVL on dehydration of DMTHF was further investigated by varying partial pressure of GVL. The results in Figure 3c clearly show that the inhibition effect of GVL in DMTHF dehydration increases with the partial pressure of GVL. This observation suggests that GVL inhibits the dehydration of DMTHF, possibly by competitive adsorption on acid sites. In fact, a small fraction of GVL was found to convert to PA isomers under the reaction conditions in this study. As GVL competes for the acid sites, the surface coverage of DMTHF under different solvent feeding conditions would be influenced consequently. It is acknowledged that the effect of GVL on DMTHF dehydration may not be as simple as traditional site competition. As surface coverage of GVL increases, the consequential change in the local environment around the active site may modify adsorbate and transition-state energies. The reaction order of DMTHF dehydration with respect to GVL is −0.63 in the range of P_{GVL} = 0.3−0.6 kPa (Figure S19), but the decrease in the dehydration rate of DMTHF with respect to GVL partial pressure becomes less significant at P_{GVL} = 1.16 kPa (Figure 3c) than this dependence would predict. Therefore, in addition to saturating the surface, the presence of GVL, particularly at high partial pressures, may also create a modified solvation environment within the zeolite pores that diminishes net dehydration rates.

The change in reaction order of DMTHF dehydration with respect to DMTHF in different co-feeding experiments over MFI-140 suggests that the adsorption state is altered under these reaction conditions. The reaction orders of DMTHF dehydration with respect to DMTHF with and without co-feeding water are 0.22 and 0.34, respectively. In this case, the catalyst surface is nearly saturated by DMTHF, which suggests the strong interaction of cyclic ether with BASs. Then, co-feeding GVL increases the reaction order of DMTHF to 1.23, which suggests that the surface coverage by DMTHF in MFI-140 catalyst is reduced. This decrease in DMTHF coverage is likely due to the competitive adsorption of GVL on BAS as aforementioned. Interestingly, adding water with GVL changes the apparent reaction order with respect to P_{DMTHF} to 0.53, suggesting greater surface coverage by DMTHF. Clearly, the initial turnover frequency of hexadiene formation correlates well with apparent reaction order and therefore surface coverage of DMTHF in zeolite catalysts. It is noted that in the presence of water, protons on the zeolite framework are delocalized to form hydronium ion clusters acting as mobile BASs under these reaction conditions. As a result, the heat of adsorption of DMTHF and GVL on conventional BAS and hydronium ion cluster could be altered, leading to the different surface coverage of DMTHF in the absence and presence of water molecules inside zeolite pores.

The apparent activation energy of hexadiene formation in 2,5-hexanediol dehydration in the presence of GVL over MFI-140 with and without water co-feeding was estimated by an Arrhenius plot over the temperature range of 220−250 °C. As shown in Figure S20, the apparent activation energy of hexadiene formation over MFI-140 in the presence of water is higher than that in the absence of water. The presence of water enables a higher surface coverage by the intermediate DMTHF as shown by reaction order results in Figure 3b. As a result, the heat of adsorption of cyclic ether may be incorporated in the measured activation energy for the reaction in the presence of water, while the activation energy in the absence of water is referenced to the gas phase due to the first-order reaction. Consequently, the measured energy barrier of 2,5-hexanediol dehydration in the presence of GVL is higher when water is co-fed. The difference of activation energy in the presence and absence of water is approximately 21 kJ/mol (calculated from Figure S20), which is consistent with the calculated heat of adsorption of DMTHF in the presence of GVL and water molecules.

3.2. DFT Analysis in the Effect of GVL and Co-Fed Water on the Dehydration of DMTHF. To further investigate the inhibitory effect of GVL in the absence of co-fed water on the conversion of DMTHF, we performed DFT calculations on the energetics of molecular adsorption over the BASs. As shown in Figure 4, the Gibbs-free-energy change of

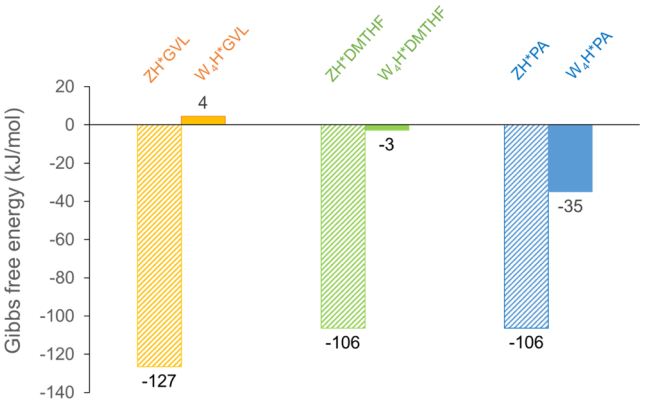

Figure 4. Gibbs free energy of adsorption of GVL, DMTHF, and PA. Z: zeolite framework; H: the proton; ZH: the framework BAS ("conventional" BAS); GVL: γ-valerolactone; DMTHF: 2,5-dimethyl tetrahydrofuran; PA: pentenoic acid isomers; W: water; W4: cluster of four water molecules; W4H: the hydronium cluster ("mobile" BAS).

GVL adsorption (−127 kJ/mol) is substantially greater than that of DMTHF adsorption (−106 kJ/mol). Accordingly, the equilibrium constant for GVL adsorption is about 100 times higher than that for DMTHF (Table S2). The result suggests that GVL should dominate the surface coverage; the hexadiene formation from DMTHF in the presence of GVL, compared to that in the solvent-free condition, will exhibit a decreased TOF and an increase in the reaction order with respect to DMTHF. In addition, Figure 4 shows that PA isomers, which are the ring-opening products of GVL, could also suppress the surface coverage of DMTHF due to their comparable Gibbs free energies of adsorption (Table S2). These findings are consistent with the experimental observations depicted in Figures 1c and S11.

To understand the mechanism by which co-fed water remediates the surface coverage of DMTHF and thus improves the TOF of hexadiene formation and why it only works in the presence of GVL but not in the DMTHF-alone system, we performed DFT calculations on the adsorption of relevant species in the presence of four water molecules per acid site (based on the experimental measurement of 4 mol of water/mole of acid sites). It is demonstrated that the proton on the

https://doi.org/10.1021/acscatal.2c05303
ACS Catal. 2023, 13, 1503−1512

zeolite framework (or "conventional" BAS) could be transferred into the cluster of four co-fed water molecules, which results in the formation of a "mobile" proton (Figure S21d). This phenomenon has been observed when more than two water molecules are introduced per site.[55]

On the mobile proton, the competitive adsorption of GVL could be further suppressed as compared to conventional BAS. As depicted in Figures 4 and S22, GVL adsorption on the hydronium cluster exhibits an almost thermoneutral Gibbs free energy similar to DMTHF. As a result, the equilibrium constant of GVL adsorption on the mobile proton is decreased (Table S2), which leads to a higher coverage of DMTHF, a reduced reaction order of DMTHF, and an improved TOF of hexadiene formation. It should be noted that with the reaction in the GVL solvent, the rate of hexadiene formation in the presence of water increases despite an increased apparent activation barrier. This result could be attributed to a larger entropy change when the reaction proceeds through a looser transition state in the presence of water, which should be associated with a much weaker adsorption of DMTHF on the hydronium cluster than on framework proton in the presence of GVL. Another possible explanation for this observation could be the greater entropy change due to the replacement of the water cluster by DMTHF upon its adsorption. These findings are consistent with experimental observations shown in Figure 1c. It is worth noting that, in the absence of GVL, water co-feeding shows no significant changes in the TOF of hexadiene formation (Figure 3a, Figure 3b, Figure S12), which can be attributed to the high coverage of DMTHF with and without co-fed water and similar intrinsic activation barriers in both cases.

Additional evidence to support water-induced coverage change is found in the results of experiments with co-fed PA, which is a ring-opening product of GVL. Different from GVL and DMTHF, the hydronium cluster substantially favors the adsorption of PA isomers (Table S2). This distinct effect suggests that a small amount of PA resulting from the ring-opening of GVL could quite significantly inhibit the hexadiene formation due to its competitive adsorption on the surface. This finding thus explains the experimental observation that water co-feeding is not able to promote hexadiene formation in the presence of PA (Figure S11).

3.3. Effect of Water on Dehydration of Real EVOH Polymer. The dehydration of real EVOH polymer over the solid acid catalyst at 120 °C in the presence of a polar aprotic solvent was investigated in a batch reactor. A nitrogen atmospheric environment was applied to minimize the side reactions in ambient air.

The dried solid product of EVOH dehydration over MFI-140 zeolite in GVL solvent was analyzed by FT-IR (Figure 5a,b). The FT-IR spectra of EVOH powder and dehydrated solid products after 2 h liquid-phase reaction are shown in Figure 5a with the appearance of the typical peaks such as O−H stretching at 3700−3000 cm^{-1}, C−H stretching at 3000−2700 cm^{-1}, O−H bending at 1590−1270 cm^{-1}, and C−O stretching at 1270−970 cm^{-1}. The FT-IR spectra of EVOH powder and the solid product after mixing with GVL in the absence of the catalyst are identical. After adding MFI-140 catalyst with the catalyst-to-polymer mass ratio of 1:3, we see a shift of C−O stretching peak from 1170 to 970 cm^{-1} to a higher wavenumber range of 1270−1100 cm^{-1}. This observation indicates the transformation of secondary alcohol bonding in EVOH to a more ether-like bonding with the

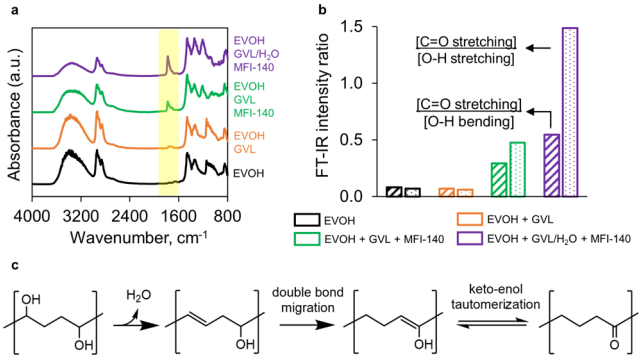

Figure 5. Dehydration of EVOH polymer. (a) FT-IR spectra of original EVOH powder and dried solid products after reactions in liquid phase. Reaction conditions: 300 mg of EVOH powder, 20 mL of the solvent, 100 mg of MFI-140, T = 120 °C, reaction time = 2 h, stirring = 600 rpm. (b) FT-IR peak intensity ratios of C═O stretching to O−H bending or O−H stretching of original EVOH powder and dried solid products after reactions in liquid phase. (c) Illustrated scheme for the formation of C═O double bonds in EVOH dehydration over the solid acid catalyst in GVL solvent.

presence of a solid acid catalyst. Another new feature showing up in FT-IR spectra with addition of MFI-140 zeolite in Figure 5a is the highlighted region of C═O stretching at 1810−1680 cm^{-1}. This C═O stretching peak is the indication of the dehydration of EVOH as explained in Figure 5c. As EVOH undergoes dehydration with the presence of MFI-140 zeolite, C═C double bonds are formed with the elimination of water molecules. The IR absorption band for C═C stretching at 1680−1600 cm^{-1} is not visible in FT-IR spectra as shown in Figure 5a, which suggests that there are sequential reactions related to these C═C double bonds. In fact, the appearance of C═O stretching band has been observed during thermal or ion-induced degradation of polyvinyl alcohol, which is attributed to double-bond migration via hydride shift mechanism, followed by keto−enol tautomerization.[56−58]

The conversion of EVOH by dehydration is indicated indirectly via FT-IR intensity ratio of C═O stretching to O−H stretching or O−H bending as shown in Figure 5b. Interestingly, adding water to the reaction mixture with the volumetric ratio of GVL/H_2O = 9:1 has shown a significant enhancement in these IR band intensity ratios. This observation implies that the positive effect of water on 2,5-hexanediol model compound is also applicable to the real EVOH dehydration over MFI-140 zeolite in the presence of GVL solvent.

4. CONCLUSIONS

Water shows an enhancement effect on EVOH polymer dehydration over MFI-140 in the presence of GVL solvent, which was investigated via the study of the model compound. The reaction pathway of 2,5-hexanediol dehydration over H-ZSM-5 zeolites was found to proceed via DMTHF intermediate to form hexadiene isomers. It was found that surface coverage of the intermediate ether (DMTHF) decreases in the presence of GVL due to the competitive adsorption of GVL, a portion of which undergoes ring-opening to form PAs. In the absence of GVL solvent, water does not influence the dehydration of the intermediate ether. Interestingly, the co-presence of water would mitigate the inhibition effect of GVL and improve the formation of hexadienes. The presence of water inside zeolite pores is known to facilitate

https://doi.org/10.1021/acscatal.2c05303
ACS Catal. 2023, 13, 1503−1512

delocalization of BASs to form hydronium ion clusters which act as mobile acid sites. Therefore, the accessibility of the intermediate ether (DMTHF) to acid sites in the presence of GVL is improved when water is co-fed as indicated by the concomitant increase in the apparent reaction order with respect to the ether. As a result, the inhibition effect of GVL is mitigated by the formation of hydronium ion clusters in the presence of water, leading to a higher rate of hexadiene formation. These findings provide mechanistic insights to guide the design of robust catalytic systems for the real EVOH polymer dehydration as well as mixed plastics recycling.

■ ASSOCIATED CONTENT

Supporting Information

The Supporting Information is available free of charge at https://pubs.acs.org/doi/10.1021/acscatal.2c05303.

Catalyst characterization, product yields and formation rates versus reaction time on stream, effect of co-feeding water on 2,5-hexanediol dehydration in the presence of GVL, GVL conversion in the presence of water, PA co-feeding experiment, effect of intermittent co-feeding water on DMTHF dehydration, reaction order of DMTHF dehydration with respect to DMTHF and GVL in different co-feeding experiments, activation energy of 2,5-hexanediol dehydration, statistical thermodynamics calculation, energetics of adsorptions, optimized structures over the framework BAS, and optimized structures over the hydronium cluster (PDF)

■ AUTHOR INFORMATION

Corresponding Author

Steven P. Crossley − *School of Chemical, Biological and Materials Engineering, University of Oklahoma, Norman, Oklahoma 73019, United States;* orcid.org/0000-0002-1017-9839; Phone: (405) 325-5930; Email: stevencrossley@ou.edu; Fax: (405) 325-5813

Authors

Han K. Chau − *School of Chemical, Biological and Materials Engineering, University of Oklahoma, Norman, Oklahoma 73019, United States;* orcid.org/0000-0003-3172-0257

Quy P. Nguyen − *School of Chemical, Biological and Materials Engineering, University of Oklahoma, Norman, Oklahoma 73019, United States*

Ana Carolina Jerdy − *School of Chemical, Biological and Materials Engineering, University of Oklahoma, Norman, Oklahoma 73019, United States*

Dai-Phat Bui − *School of Chemical, Biological and Materials Engineering, University of Oklahoma, Norman, Oklahoma 73019, United States;* orcid.org/0000-0002-3886-9022

Lance L. Lobban − *School of Chemical, Biological and Materials Engineering, University of Oklahoma, Norman, Oklahoma 73019, United States*

Bin Wang − *School of Chemical, Biological and Materials Engineering, University of Oklahoma, Norman, Oklahoma 73019, United States;* orcid.org/0000-0001-8246-1422

Complete contact information is available at: https://pubs.acs.org/10.1021/acscatal.2c05303

Notes

The authors declare no competing financial interest.

■ ACKNOWLEDGMENTS

The authors are grateful for the support from the National Science Foundation under grant no. EFRI E3P-2029394 to carry out this research. The computations were performed at the OU Supercomputing Center for Education & Research and the National Energy Research Scientific Computing Center (NERSC), a U.S. Department of Energy Office of Science User Facility. B.W. would like to thank support from the U.S. Department of Energy, Basic Energy Sciences (Grant DE-SC0018284).

■ REFERENCES

(1) Niaounakis, M.*Recycling of Flexible Plastic Packaging*; William Andrew, 2019; p 466.

(2) Garcia, J. M.; Robertson, M. L. The future of plastics recycling. *Science* **2017**, *358*, 870−872.

(3) Jehanno, C.; Alty, J. W.; Roosen, M.; De Meester, S.; Dove, A. P.; Chen, E. Y.-X.; Leibfarth, F. A.; Sardon, H. Critical advances and future opportunities in upcycling commodity polymers. *Nature* **2022**, *603*, 803−814.

(4) Korley, L. T.; Epps, T. H.; Helms, B. A.; Ryan, A. J. Toward polymer upcycling—adding value and tackling circularity. *Science* **2021**, *373*, 66−69.

(5) Martín, A. J.; Mondelli, C.; Jaydev, S. D.; Pérez-Ramírez, J. Catalytic processing of plastic waste on the rise. *Chem* **2021**, *7*, 1487−1533.

(6) Ellis, L. D.; Rorrer, N. A.; Sullivan, K. P.; Otto, M.; McGeehan, J. E.; Román-Leshkov, Y.; Wierckx, N.; Beckham, G. T. Chemical and biological catalysis for plastics recycling and upcycling. *Nat. Catal.* **2021**, *4*, 539−556.

(7) Vollmer, I.; Jenks, M. J.; Roelands, M. C.; White, R. J.; Harmelen, T.; Wild, P.; Laan, G. P.; Meirer, F.; Keurentjes, J. T.; Weckhuysen, B. M. Beyond mechanical recycling: Giving new life to plastic waste. *Angew. Chem., Int. Ed.* **2020**, *59*, 15402−15423.

(8) Roy, P. S.; Garnier, G.; Allais, F.; Saito, K. Strategic approach towards plastic waste valorization: challenges and promising chemical upcycling possibilities. *ChemSusChem* **2021**, *14*, 4007−4027.

(9) Chen, H.; Wan, K.; Zhang, Y.; Wang, Y. Waste to Wealth: Chemical Recycling and Chemical Upcycling of Waste Plastics for a Great Future. *ChemSusChem* **2021**, *14*, 4123.

(10) Hou, Q.; Zhen, M.; Qian, H.; Nie, Y.; Bai, X.; Xia, T.; Laiq Ur Rehman, M. L. U.; Li, Q.; Ju, M. Upcycling and catalytic degradation of plastic wastes. *Cell Rep. Phys. Sci.* **2021**, *2*, 100514.

(11) Chen, X.; Wang, Y.; Zhang, L. Recent progress in the chemical upcycling of plastic wastes. *ChemSusChem* **2021**, *14*, 4137−4151.

(12) Horodytska, O.; Valdés, F. J.; Fullana, A. Plastic flexible films waste management−A state of art review. *Waste Manage.* **2018**, *77*, 413−425.

(13) Sánchez-Rivera, K. L.; Zhou, P.; Kim, M. S.; González Chávez, L. D.; Grey, S.; Nelson, K.; Wang, S.-C.; Hermans, I.; Zavala, V. M.; Van Lehn, R. C.; Huber, G. W. Reducing Antisolvent Use in the STRAP Process by Enabling a Temperature-Controlled Polymer Dissolution and Precipitation for the Recycling of Multilayer Plastic Films. *ChemSusChem* **2021**, *14*, 4317−4329.

(14) Walker, T. W.; Frelka, N.; Shen, Z.; Chew, A. K.; Banick, J.; Grey, S.; Kim, M. S.; Dumesic, J. A.; Van Lehn, R. C.; Huber, G. W. Recycling of multilayer plastic packaging materials by solvent-targeted recovery and precipitation. *Sci. Adv.* **2020**, *6*, No. eaba7599.

(15) Corma, A. Inorganic solid acids and their use in acid-catalyzed hydrocarbon reactions. *Chem. Rev.* **1995**, *95*, 559−614.

(16) Macht, J.; Janik, M. J.; Neurock, M.; Iglesia, E. Mechanistic consequences of composition in acid catalysis by polyoxometalate keggin clusters. *J. Am. Chem. Soc.* **2008**, *130*, 10369−10379.

(17) Chen, F.; Shetty, M.; Wang, M.; Shi, H.; Liu, Y.; Camaioni, D. M.; Gutiérrez, O. Y.; Lercher, J. A. Differences in Mechanism and Rate of Zeolite-Catalyzed Cyclohexanol Dehydration in Apolar and Aqueous Phase. *ACS Catal.* **2021**, *11*, 2879−2888.

(18) Zhi, Y.; Shi, H.; Mu, L.; Liu, Y.; Mei, D.; Camaioni, D. M.; Lercher, J. A. Dehydration Pathways of 1-Propanol on HZSM-5 in the Presence and Absence of Water. *J. Am. Chem. Soc.* **2015**, *137*, 15781−15794.
(19) Vjunov, A.; Wang, M.; Govind, N.; Huthwelker, T.; Shi, H.; Mei, D.; Fulton, J. L.; Lercher, J. A. Tracking the chemical transformations at the Brønsted acid site upon water-induced deprotonation in a zeolite pore. *Chem. Mater.* **2017**, *29*, 9030−9042.
(20) Wang, M.; Jaegers, N. R.; Lee, M.-S.; Wan, C.; Hu, J. Z.; Shi, H.; Mei, D.; Burton, S. D.; Camaioni, D. M.; Gutiérrez, O. Y.; Glezakou, V.-A.; Rousseau, R.; Wang, Y.; Lercher, J. A. Genesis and stability of hydronium ions in zeolite channels. *J. Am. Chem. Soc.* **2019**, *141*, 3444−3455.
(21) Pfriem, N.; Hintermeier, P. H.; Eckstein, S.; Kim, S.; Liu, Q.; Shi, H.; Milakovic, L.; Liu, Y.; Haller, G. L.; Baráth, E.; Liu, Y.; Lercher, J. A. Role of the ionic environment in enhancing the activity of reacting molecules in zeolite pores. *Science* **2021**, *372*, 952−957.
(22) DeWilde, J. F.; Chiang, H.; Hickman, D. A.; Ho, C. R.; Bhan, A. Kinetics and mechanism of ethanol dehydration on γ-Al_2O_3: the critical role of dimer inhibition. *ACS Catal.* **2013**, *3*, 798−807.
(23) Bates, J. S.; Bukowski, B. C.; Greeley, J.; Gounder, R. Structure and solvation of confined water and water−ethanol clusters within microporous Brønsted acids and their effects on ethanol dehydration catalysis. *Chem. Sci.* **2020**, *11*, 7102−7122.
(24) Alonso, D. M.; Wettstein, S. G.; Dumesic, J. A. Gamma-valerolactone, a sustainable platform molecule derived from lignocellulosic biomass. *Green Chem.* **2013**, *15*, 584−595.
(25) Chau, H. K.; Resasco, D. E.; Do, P.; Crossley, S. P. Acylation of m-cresol with acetic acid supported by in situ ester formation on H-ZSM-5 zeolites. *J. Catal.* **2022**, *406*, 48−55.
(26) Kresse, G.; Furthmüller, J. Efficient iterative schemes for ab initio total-energy calculations using a plane-wave basis set. *Phys. Rev. B: Condens. Matter Mater. Phys.* **1996**, *54*, 11169.
(27) Blöchl, P. E. Projector augmented-wave method. *Phys. Rev. B: Condens. Matter* **1994**, *50*, 17953.
(28) Kresse, G.; Joubert, D. From ultrasoft pseudopotentials to the projector augmented-wave method. *Phys. Rev. B: Condens. Matter Mater. Phys.* **1999**, *59*, 1758.
(29) Perdew, J. P.; Burke, K.; Ernzerhof, M. Generalized gradient approximation made simple. *Phys. Rev. Lett.* **1996**, *77*, 3865.
(30) Grimme, S.; Antony, J.; Ehrlich, S.; Krieg, H. A consistent and accurate ab initio parametrization of density functional dispersion correction (DFT-D) for the 94 elements H-Pu. *J. Chem. Phys.* **2010**, *132*, 154104.
(31) Dauenhauer, P. J.; Abdelrahman, O. A. A universal descriptor for the entropy of adsorbed molecules in confined spaces. *ACS Cent. Sci.* **2018**, *4*, 1235−1243.
(32) De Moor, B. A.; Ghysels, A.; Reyniers, M.-F.; Van Speybroeck, V.; Waroquier, M.; Marin, G. B. Normal mode analysis in zeolites: toward an efficient calculation of adsorption entropies. *J. Chem. Theory Comput.* **2011**, *7*, 1090−1101.
(33) Cramer, C. J.*Essentials of Computational Chemistry: Theories and Models*, 2nd ed.; John Wiley & Sons, 2004; p 624.
(34) van Koningsveld, H. v. High-temperature (350 K) orthorhombic framework structure of zeolite H-ZSM-5. *Acta Crystallogr., Sect. B: Struct. Sci.* **1990**, *46*, 731−735.
(35) Zeets, M.; Resasco, D. E.; Wang, B. Enhanced chemical activity and wettability at adjacent Brønsted acid sites in HZSM-5. *Catal. Today* **2018**, *312*, 44−50.
(36) Chen, K.; Horstmeier, S.; Nguyen, V. T.; Wang, B.; Crossley, S. P.; Pham, T.; Gan, Z.; Hung, I.; White, J. L. Structure and catalytic characterization of a second framework Al (IV) site in zeolite catalysts revealed by NMR at 35.2 T. *J. Am. Chem. Soc.* **2020**, *142*, 7514−7523.
(37) Chen, K.; Abdolrahmani, M.; Horstmeier, S.; Pham, T. N.; Nguyen, V. T.; Zeets, M.; Wang, B.; Crossley, S.; White, J. L. Brønsted−Brønsted synergies between framework and noncrystalline protons in zeolite H-ZSM-5. *ACS Catal.* **2019**, *9*, 6124−6136.
(38) Abdelrahman, O. A.; Park, D. S.; Vinter, K. P.; Spanjers, C. S.; Ren, L.; Cho, H. J.; Zhang, K.; Fan, W.; Tsapatsis, M.; Dauenhauer, P. J. Renewable isoprene by sequential hydrogenation of itaconic acid and dehydra-decyclization of 3-methyl-tetrahydrofuran. *ACS Catal.* **2017**, *7*, 1428−1431.
(39) Abdelrahman, O. A.; Park, D. S.; Vinter, K. P.; Spanjers, C. S.; Ren, L.; Cho, H. J.; Vlachos, D. G.; Fan, W.; Tsapatsis, M.; Dauenhauer, P. J. Biomass-derived butadiene by dehydra-decyclization of tetrahydrofuran. *ACS Sustainable Chem. Eng.* **2017**, *5*, 3732−3736.
(40) Li, S.; Abdelrahman, O. A.; Kumar, G.; Tsapatsis, M.; Vlachos, D. G.; Caratzoulas, S.; Dauenhauer, P. J. Dehydra-decyclization of tetrahydrofuran on H-ZSM5: mechanisms, pathways, and transition state entropy. *ACS Catal.* **2019**, *9*, 10279−10293.
(41) Kumar, G.; Liu, D.; Xu, D.; Ren, L.; Tsapatsis, M.; Dauenhauer, P. J. Dehydra-decyclization of 2-methyltetrahydrofuran to pentadienes on boron-containing zeolites. *Green Chem.* **2020**, *22*, 4147−4160.
(42) Kumbhalkar, M. D.; Buchanan, J. S.; Huber, G. W.; Dumesic, J. A. Ring opening of biomass-derived cyclic ethers to dienes over silica/alumina. *ACS Catal.* **2017**, *7*, 5248−5256.
(43) Bond, J. Q.; Martin Alonso, D.; West, R. M.; Dumesic, J. A. γ-Valerolactone ring-opening and decarboxylation over SiO_2/Al_2O_3 in the presence of water. *Langmuir* **2010**, *26*, 16291−16298.
(44) Janda, A.; Bell, A. T. Effects of Si/Al ratio on the distribution of framework Al and on the rates of alkane monomolecular cracking and dehydrogenation in H-MFI. *J. Am. Chem. Soc.* **2013**, *135*, 19193−19207.
(45) Dědeček, J.; Tabor, E.; Sklenak, S. Tuning the aluminum distribution in zeolites to increase their performance in acid-catalyzed reactions. *ChemSusChem* **2019**, *12*, 556−576.
(46) Song, C.; Chu, Y.; Wang, M.; Shi, H.; Zhao, L.; Guo, X.; Yang, W.; Shen, J.; Xue, N.; Peng, L.; Ding, W. Cooperativity of adjacent Brønsted acid sites in MFI zeolite channel leads to enhanced polarization and cracking of alkanes. *J. Catal.* **2017**, *349*, 163−174.
(47) Mlinar, A. N.; Zimmerman, P. M.; Celik, F. E.; Head-Gordon, M.; Bell, A. T. Effects of Brønsted-acid site proximity on the oligomerization of propene in H-MFI. *J. Catal.* **2012**, *288*, 65−73.
(48) Di Iorio, J. R.; Nimlos, C. T.; Gounder, R. Introducing catalytic diversity into single-site chabazite zeolites of fixed composition via synthetic control of active site proximity. *ACS Catal.* **2017**, *7*, 6663−6674.
(49) Kester, P. M.; Crum, J. T.; Li, S.; Schneider, W. F.; Gounder, R. Effects of Brønsted acid site proximity in chabazite zeolites on OH infrared spectra and protolytic propane cracking kinetics. *J. Catal.* **2021**, *395*, 210−226.
(50) Jones, A. J.; Carr, R. T.; Zones, S. I.; Iglesia, E. Acid strength and solvation in catalysis by MFI zeolites and effects of the identity, concentration and location of framework heteroatoms. *J. Catal.* **2014**, *312*, 58−68.
(51) Ong, L. H.; Dömök, M.; Olindo, R.; van Veen, A. C.; Lercher, J. A. Dealumination of HZSM-5 via steam-treatment. *Microporous Mesoporous Mater.* **2012**, *164*, 9−20.
(52) Bond, J. Q.; Jungong, C. S.; Chatzidimitriou, A. Microkinetic analysis of ring opening and decarboxylation of γ-valerolactone over silica alumina. *J. Catal.* **2016**, *344*, 640−656.
(53) Gupta, S.; Arora, R.; Sinha, N.; Alam, M. I.; Haider, M. A. Mechanistic insights into the ring-opening of biomass derived lactones. *RSC Adv.* **2016**, *6*, 12932−12942.
(54) John, M.; Alexopoulos, K.; Reyniers, M.-F.; Marin, G. B. Reaction path analysis for 1-butanol dehydration in H-ZSM-5 zeolite: Ab initio and microkinetic modeling. *J. Catal.* **2015**, *330*, 28−45.
(55) Li, G.; Wang, B.; Resasco, D. E. Water-mediated heterogeneously catalyzed reactions. *ACS Catal.* **2019**, *10*, 1294−1309.
(56) Hossain, U. H.; Seidl, T.; Ensinger, W. Combined in situ infrared and mass spectrometric analysis of high-energy heavy ion induced degradation of polyvinyl polymers. *Polym. Chem.* **2014**, *5*, 1001−1012.
(57) Holland, B.; Hay, J. The thermal degradation of poly (vinyl alcohol). *Polymer* **2001**, *42*, 6775−6783.

https://doi.org/10.1021/acscatal.2c05303
ACS Catal. 2023, 13, 1503−1512

(58) Thomas, P.; Guerbois, J.-P.; Russell, G.; Briscoe, B. FTIR study of the thermal degradation of poly (vinyl alcohol). *J. Therm. Anal. Calorim.* **2001**, *64*, 501−508.

https://doi.org/10.1021/acscatal.2c05303
ACS Catal. 2023, 13, 1503−1512